

**Kinetic, metabolic and macromolecular response of bacteria to chronic nanoparticle exposure in continuous culture**

Journal:	<i>Environmental Science: Nano</i>
Manuscript ID	EN-ART-03-2018-000325.R1
Article Type:	Paper
Date Submitted by the Author:	03-May-2018
Complete List of Authors:	Faghihzadeh, Fatemeh; University of Rhode Island, Civil and Environmental Engineering Anaya, Nelson; Wilkes University Astudillo-Castro, Carolina; Pontificia Universidad Catolica de Valparaiso, Food Engineering Craver, Vinka; University of Rhode Island, Civil and Environmental Engineering

## Environmental Impact

This study offers new insights of the role of the growth conditions on the bacteria response to the exposure to silver nanoparticles. Our results showed that the specific growth rate in which continuous culture of microorganism are growing determined the concentration and composition of extra-cellular substance produced in response to the exposure of nanoparticles, therefore impacting the physicochemical properties of the surfaces of the nanoparticles in each condition differently.



## Kinetic, metabolic and macromolecular response of bacteria to chronic nanoparticle exposure in continuous culture

F. Faghizadeh<sup>a</sup>, N. M. Anaya<sup>b</sup>, C. Astudillo-Castro<sup>c</sup>, and V. Oyanedel-Craver<sup>a\*</sup>

Received 00th January 20xx,  
Accepted 00th January 20xx

DOI: 10.1039/x0xx00000x

[www.rsc.org/](http://www.rsc.org/)

Nanoparticles with antimicrobial properties are used in thousands of nano-enabled consumer products. Therefore, it is important to understand the response mechanisms of bacteria that are exposed to these nanoparticles at different conditions. Moreover, it is necessary to evaluate possible microbial adaptation mechanisms. In our study, *Escherichia coli* K-12 MG1655 (*E. coli*) were grown continuously in bioreactors at two specific growth rates (0.1 h<sup>-1</sup> and 0.2 h<sup>-1</sup>) and then exposed to chronic concentrations of casein-coated silver nanoparticles (AgNPs) [1 mg/L] for about 180 generations. After initiating the injection of AgNPs, the results showed a change in growth kinetic parameters between non-exposed and exposed systems. Maximum yield ( $Y_{max}$ ) decreased by 33%, while the maintenance coefficient ( $m_s$ ) increased by 52%. This evidence was indicating the versatility of the culture to growth in the exposed conditions and even the ability to achieve a new stationary state. However, the adaptation was achieved at a metabolic cost. Comparing the concentration and composition of extra-cellular substances that were produced showed differences between the control and exposed conditions, and also between the exposed systems in the two growth conditions. In the AgNPs-exposed bioreactor (EB) growing at 0.1 h<sup>-1</sup>, AgNPs-ES complexes showed that the ratio of the area representing  $\beta$ -sheets to the area representing  $\alpha$ -helix proteins was 2.4, which implies the formation of a protein corona, while at an exposed growth rate of 0.2 h<sup>-1</sup> this ratio was < 1, indicating no protein corona. Transcriptomic results showed gene regulation in response to AgNPs exposure as a function of the specific growth rate. Batch exposure tests using the resultant cultures for each condition showed a lower inhibitory effect for the AgNPs on EB at 0.1 h<sup>-1</sup> than on control bacteria (CB) at 0.1 h<sup>-1</sup> in terms of membrane permeation and reactive oxygen species generation. Overall, our study showed that culture growth conditions significantly affects bacterial response to nanoparticle exposure. Therefore, these growth parameters should be determined and reported when performing toxicological tests.

### 1. Introduction

Antimicrobial nanoparticles are used to inhibit and deactivate unwanted microorganisms,<sup>1-3</sup> however, bacteria stress response mechanisms can hinder the efficacy of these nanoparticles.

The impact of nanoparticles on bacteria activity and growth depends on several parameters, including the physicochemical properties of the nanoparticles core and shell, bulk composition, as well as the physicochemical and physiological properties of the microorganisms.<sup>4</sup> During bacterial growth, bulk composition changes due to the consumption and production of compounds by the

bacteria. Therefore, the physicochemical characteristics of the surfaces of the nanoparticles can change through ligand capping of the organic molecules, such as thru extra-cellular substances (ES).<sup>5</sup> ES consist mainly of polysaccharides, proteins, nucleic acids, and lipids.<sup>6,7</sup> Previous studies have shown that the concentration and composition of ES changes with variation in the growth rates of microbial cultures.<sup>7,8</sup> Therefore, the interactions with nanoparticles may also change nanoparticle surface properties. To the best of our knowledge, this has not been previously assessed.

Studies of the interaction of AgNPs with bacteria are usually conducted in batch and/or continuous bioreactors.<sup>1,4,9</sup> In batch reactors, the growth rate of the bacteria culture changes over time due to the uptake of the substrate and the release of metabolic products. Additionally, there are four distinct growth phases that can be distinguished in batch cultures: lag, exponential or log, stationary, and death. Each of these phases is associated with both bulk and physiological bacterial changes.<sup>10</sup>

<sup>a</sup> Department of Civil and Environmental Engineering, Bliss hall 203, University of Rhode Island, Kingston, RI, 02881, USA. E-mail: Faghizadeh@uri.edu; craver@uri.edu. Phone: (401)-874-2784. Fax: (401)-874-2786.

<sup>b</sup> Department of Environmental Engineering, Earth Science and Geology, Wilkes University, Wilkes-Barre, PA 18701, USA. Email: nelson.anaya@wilkes.edu

<sup>c</sup> School of Food Engineering, Pontificia Universidad Católica de Valparaíso, 716 Waddington, Playa Ancha, Valparaíso 2360100, Chile. E-mail: carolina.astudillo@pucv.cl

† Electronic Supplementary Information (ESI) available. See DOI: 10.1039/x0xx00000x

Therefore, it can be inferred that the physicochemical properties of the nanoparticles will also likely change throughout the experimental period.

Continuous reactors can be used to overcome these limitations. These reactors can achieve steady-state conditions where the concentration of the growth-controlling substrate and density of the culture do not change significantly with time.<sup>11</sup> Continuous cultures have been used extensively to study bacteria stress response and to investigate the development of antibiotic resistance.<sup>12–14</sup> In a previous study, we compared bacteria exposed to pulses of AgNPs using continuous and batch reactors, and our results showed that in terms of membrane permeability, there were marked differences between both conditions.<sup>1</sup> Numerous studies have reported the effects of AgNPs in terms of multiple parameters related to cell viability.<sup>15,4,16,17</sup> However, to the best of our knowledge, changes in the physicochemical properties of the nanoparticles at different continuous culture conditions have not been reported.

Additionally, most studies have focused on the antimicrobial effects of nanoparticles, but have not considered that in nature, microorganisms grow in the presence of inhibitors. Therefore, in addition to nutrient uptake, growth may be controlled by the presence of anthropogenic inhibitors, such as nanoparticles.<sup>18–20</sup> Therefore, assessing the impact of nanoparticles on kinetic parameters that commonly occur in the ecological context is extremely important.

The main objective of this study was to elucidate the impact of bacterial growth conditions and their response to chronic exposure to silver nanoparticles. We used continuous bioreactors to determine the inhibitory effect of nanoparticles in terms of kinetic parameters, nanoparticle-ES interactions, and transcriptomic analysis. Additionally, culture samples from the effluent of the exposed bioreactor (EB) and control (CB) bioreactors were re-cultured in batch mode, and then acutely exposed to AgNPs in order to compare membrane permeation, respiration activity, and reactive oxygen species (ROS) generation responses.

## 2. Material and Methods

### 2.1. Materials

A non-pathogenic strain of *Escherichia coli* K-12 strain MG1655 (ATCC 700926) (*E. coli*) was selected for this study. *E. coli* is a Gram-negative bacterium that has been extensively used in nano-toxicological studies.<sup>9,21</sup> The reagents used to prepare the M9 minimal growth media for the bacteria<sup>22</sup> included: M9 minimal salts, glucose solution (BioUltra, ~20% in DI water), calcium chloride, thiamine hydrochloride and magnesium sulfate heptahydrate; and a phosphate buffer solution (PBS) containing monobasic potassium phosphate, dibasic potassium phosphate and ethylenediaminetetraacetic acid. A glucose

(HK) assay kit (GAHK201KT) was purchased from Sigma Aldrich and used as received. SYTO 9 and propidium iodide for cell membrane permeation were purchased from Invitrogen. Standard casein-coated AgNPs were obtained from Argenol Laboratories (Spain). This type of nanoparticles have been used in previous studies due to their antimicrobial properties.<sup>15</sup>

ROS was measured with a Dichlorofluorescein diacetate (DCFDA) Cellular ROS Detection Assay Kit from Abcam (ab113851). A Synergy TM MX microplate reader (BIOTEK, VT) was used for the batch exposure experiment.

### 2.2. Methods

**2.2.1. Bacteria culture.** In this study, we used a slightly modified version of the multiplex bioreactor system from our previous study<sup>1</sup> (Figure S4 in the ESI). The vessels were fed with sterile M9 minimal medium adjusted to pH 7.2 and air (airflow of 1.5 L/min). A peristaltic pump provided a flow rate of 0.1 mL/min to achieve a growth rate of 0.1 h<sup>-1</sup> in one run, while 0.14 mL/min was used to achieve the 0.2 h<sup>-1</sup> condition in the second run. Each run consisted of four bioreactors inoculated with 300 µL of *E. coli* inoculum (optical density at 600 nm = 1.8) and two bioreactors as blanks with only M9 minimal media. After reaching steady state in terms of bacteria optical density (OD), the four bioreactors were inoculated with *E. coli*, and two bioreactors were injected continuously with AgNPs using syringe pumps (model 100 from Kd-Scientific) (exposed bioreactors, EB), while the other two bioreactors were fed with only M9 medium as controls (CB). Subsequently, all of the bioreactors were operated for at least 32 hours. Samples were taken from each reactor every 4 hours, centrifuged and the supernatant was stored at -20 °C to extract ES<sup>23</sup> and to determine glucose concentration.<sup>24</sup> OD600 of the resuspended pellet in 10% PBS was measured to determine bacteria concentration using a UV Vis-spectrophotometer. The resuspended pellets from all bioreactors were stored in sterile glycerol at -20°C and used for the regrowth and toxicity analysis described in Section 2.5.

**2.2.2. Kinetic parameter calculations.** The maximum specific growth rate ( $\mu_{max}$ ) of *E. coli* and washout dilution rate value were determined using a methodology found in the literature<sup>25,26</sup> (Details in ESI).  $\mu_{max}$  was 0.21 h<sup>-1</sup>, while the wash out dilution rate was 0.3 h<sup>-1</sup> (Figure S2 in the ESI). The operational conditions in terms of specific growth rate selected for this study were to 0.1 h<sup>-1</sup> and 0.2 h<sup>-1</sup>.

Biomass concentration was followed by measuring OD600 according to previously published protocols.<sup>27</sup> Additionally, dry biomass weight was obtained for all bioreactors and normalized based on the internal volume of the continuous bioreactor vessels.

Glucose concentration (*S*) in the bioreactors was determined thru a glucose (HK) assay reagent<sup>24</sup> following manufacturer instructions.

The Monod equation was used to determine the saturation constant ( $K_s$ ), yield coefficient ( $Y_{x/s}$ ), maximum yield ( $Y_{max}$ ), and maintenance coefficient ( $m_s$ ) in the bioreactors at steady state

conditions.<sup>28</sup> The  $K_s$  for glucose was determined using Equation 1 from continuous bioreactor theory.<sup>26,28</sup>

$$K_s = S \left( \frac{\mu_{\max}}{\mu} - 1 \right) \quad \text{Equation 1}$$

$K_s$  is the substrate saturation constant (mmol/L),  $S$  is the outlet substrate concentration (mmol),  $\mu$  is specific growth rate ( $\text{h}^{-1}$ ), and  $\mu_{\max}$  is maximum specific growth rate ( $\text{h}^{-1}$ ).

$Y_{x/s}$  was determined by dividing biomass concentration (normalized mg dry weight cell) per mmol consumed substrate.<sup>27,29</sup> Furthermore,  $Y_{\max}$  and  $m_s$  were obtained from the regression parameters of Equation 2.<sup>29</sup>

$$\frac{1}{Y_{x/s}} = \frac{1}{Y_{\max}} + \frac{m_s}{\mu} \quad \text{Equation 2}$$

### 2.3. Nanoparticles-ES interaction analysis

**2.3.1. Nanoparticle Characterization.** AgNPs were continuously injected into each bioreactor to achieve a concentration of 1 mg/L inside the exposed bioreactors. (Figure S4 and details provided in ESI).

The nanoparticle hydrodynamic diameter size distribution and zeta potential ( $\zeta$ ) of the nano-suspensions were determined by using dynamic light scattering (DLS) using a Zetasizer Nano (Malvern, ZEN 3600). Inductively-coupled plasma spectroscopy (ICP-OES optima 3100, Perkin Elmer) and inductively coupled plasma mass spectrometry (iCAP Q ICP-MS) were used to measure the concentrations of AgNPs and silver ions ( $\text{Ag}^+$ ). The ionic release from AgNPs at each condition was quantified as Anaya *et al.*,<sup>1</sup> Ag ions released was quantified for the conditions: AgNPs with ES (from continuous bioreactors), AgNPs with M9 minimal medium, and AgNPs with distilled water (control). Digestion in 2% nitric acid was required for all samples before analysis.

**2.3.2. Cryogenic transmission electron microscopy.** Nanoparticle suspensions were characterized by transmission electron microscopy (cryo-TEM). Also, the interaction between AgNPs-ES and formation of the protein corona on the nanoparticles surface were monitored by cryo-TEM during several exposure times (0 h, 8 h, and 32 h). Sample for cryo-TEM were verified using a Vitrobot (FEI Company).<sup>30</sup> Quantifoil grids with 2 mm holey-carbon on 200 square mesh copper (Electron Microscopy Sciences, Hat-field, PA) were used for specimen preparation. Imaging was done with a JEOL JEM-2100F TEM (Peabody, MA) in a cooled stage (model 915, Gatan Inc., Pleasanton, CA). ImageJ software was used for image analysis.

**2.3.3. ES quantification and characterization.** Initially, ES was separated from the bacterial culture suspension of the continuous bioreactor using a previously described methodology by Seo and Bailey.<sup>23</sup>

Dried ES were characterized using ATR-FTIR (Nicolet iS50 FTIR, Thermo Scientific). Spectra of the samples were the result of 256 scans with a resolution of  $4 \text{ cm}^{-1}$  in the  $1800\text{-}900 \text{ cm}^{-1}$  spectral range (Omnic software, Thermo Scientific) and processed using MATLAB (MathWorks Software). Hierarchical cluster analysis (HCA) was applied to discriminate the compositional differences between the ATR-FTIR spectra of ES

from exposed and control bioreactors at the various tested conditions.<sup>31,32</sup> For HCA, a data set was collected from the pairwise similarity coefficients of all spectra as a matrix of correlation coefficients, which contains the total number of spectra ( $N$  entries).<sup>33,34</sup> Between two spectra, each correlation coefficient can range from 0.0 for completely different spectra to 1.0 for identical spectra. Similar spectra were obtained by recalculation of the correlation matrix. Then identical spectra were merged into a new object and the merging process repeated until all spectra were combined into a small number of clusters.

Thermogravimetric analysis (TGA) of dried ES was performed in a thermogravimetric apparatus with  $\text{N}_2$  atmosphere by using a TA instrument Q500 TGA following a previously reported methodology.<sup>35</sup> Data were also obtained from the first derivative of the TGA line. Raw TGA data were smoothed by a moving average and Gaussian fit to the first derivative of smooth data was found using MATLAB software.

Formation of protein corona on the AgNPs surface was determined by using the ATR-FTIR.<sup>36</sup> It was assumed that the observed peak is the summation of two Gaussian functions representing a  $\beta$  sheet and  $\alpha$  helix structure.<sup>2,36</sup> Coefficients for these functions were determined by a parametric fitting of the data by MATLAB on the observed peak at a range of  $1800\text{-}1550 \text{ cm}^{-1}$ . After subtraction of the protein from the casein layer of AgNPs, the ratio between areas under a  $\beta$  sheet to the  $\alpha$  helix structure of proteins was altered after corona formation.<sup>35</sup> ES without AgNPs was exposed to different concentrations of AgNPs to validate protein corona formation onto a AgNPs surface.

### 2.4. Reverse-Transcription Quantitative Polymerase Chain Reaction (RT-qPCR)

Reverse transcript (RT)-qPCR is a valuable tool widely used for analysis of gene expression.<sup>3,37-40</sup> Previously, dominant genes have been identified as responding to AgNPs inhibitory effects, including by the outer membrane porin (*ompF*), copper efflux oxidase (*cueO*), copper/silver efflux system (*cusA*), and copper transporter (*copA*) genes.<sup>4,21</sup> These genes are responsible for the following metabolic pathways: outer membrane porin F, oxidizes model substrate dimethoxyphenol, silver and copper efflux of membrane transporter, and the silver-translocating P-type ATPase efflux pump.<sup>21</sup> A previous report also showed that at the transcriptional level, fatty acid synthesis were inhibited by AgNPs inhibitory effects,<sup>38</sup> hence, we also considered expression of the beta hydroxydecanoyl thioester dehydrase (*FabR*) gene that regulates *E. coli* fatty acid synthesis.<sup>41</sup> In addition, we also determined the expression of glucose 6-phosphate dehydrogenase (*zwf*) and capsular polysaccharide (*cpsB*) regulons as they impact the respiration metabolic pathway,<sup>37</sup> as well as colanic acid and capsular polysaccharide biosynthesis.<sup>42</sup>

For real-time quantitative polymerase chain reaction (RT-qPCR) determination, samples from the effluent of the bioreactor were collected in tubes containing a RNAlater solution (Ambion Inc. Austin, TX). Total RNA extraction was

performed using a PureLink™ RNA Mini Kit (Ambion Inc. Austin, TX). Total RNA concentration was quantified by NanoDrop. In order to obtain pure RNA and reduce genomic DNA contamination, we treated the extracted RNA with DNase free from a Maxima First Strand cDNA Synthesis kit (Thermo Fisher Scientific, Waltham, MA). Then first strand cDNA was synthesized by using DNase free RNA and random primers according to the protocol of the Maxima First Strand cDNA Synthesis kit (Thermo Fisher Scientific, Waltham, MA). Running the reactions without cDNA produced negative controls. The National Center for Biotechnology Information (NCBI) was used to determine the gene sequences and to design gene-specific real-time primers, which was done by an OligoAnalyzer 3.1 tool available from the Integrated DNA Technologies website (<https://www.idtdna.com/calc/analyzer>) (details in the ESI). Primer sequences are listed in Table S4 of the ESI. The specificity of the designed primers was checked in NCBI to ensure that their binding sites are unique in the genome.

Quantification of cDNA was performed by using SYBR Green PCR Master Mix (Applied Biosystems). Two replicates per treatment were considered for RT-qPCRs using the cDNA. A Comparative Cycle threshold ( $C_T$ ) method ( $\Delta\Delta C_T$ ) was used to perform the calculations. The  $C_T$  of the target genes was normalized with the  $C_T$  of the *rrsB* to obtain its  $\Delta C_T$ . The values of  $\Delta C_T$  of the target genes were further normalized with the  $\Delta C_T$  of the control cells (*i.e.*, non-exposed cells), the result of which generated the final data set ( $\Delta\Delta C_T$ ) (details provided in ESI).<sup>21,43</sup>

### 2.5. Comparison of cultures to acute exposure to AgNPs

Samples were collected from the effluent of bioreactors EB and CB at 92 hours and 60 hours for runs with specific growth rates of  $0.1 \text{ h}^{-1}$  and  $0.2 \text{ h}^{-1}$ , respectively. Bacteria from the samples were harvested and exposed to two concentrations of AgNPs (1 mg/L and 10 mg/L) to compare the response of the resultant EB and CB cultures for each condition in terms of respirometric activity, membrane permeation and ROS production.

**2.5.1. Respirometric analysis.** Cell respiration was quantified in non-growing conditions (media consisting of a PBS solution and glucose, but without other nutrients), to compare electron transport activity due to aerobic metabolism of the carbon source. Respiration activity was determined through the reduction of tetrazolium dye<sup>44</sup> by measuring absorbance at 590 nm every 0.25 hour for 5 hours.

**2.5.2. Membrane permeation analysis.** The membrane permeation of *E. coli* was determined using a BacLight kit (propidium iodide and SYTO 9) with a microplate reader. Propidium iodide intercalates to the DNA only when the membrane is disrupted, while SYTO 9 indicates intact membranes.<sup>44</sup> The green/red fluorescence ratio between the EB and CB at the given AgNPs concentration (1 mg/L and 10 mg/L) was calculated as previously reported.<sup>44</sup>

**2.5.3. ROS generation measurement using 2',7' - dichlorofluorescein diacetate (DCFH-DA).** The reaction between DCFDA and ROS produced fluorescent product 2',7' -

dichlorofluorescein (DCF). An oxidation-sensitive fluorescent probe 2',7' -dichlorofluorescein diacetate (DCFH-DA) was measured for ROS. Non-fluorescent 2',7' -dichlorofluorescein diacetate (DCFDA) was formed by deacetylation of cellular esterases.<sup>37</sup> The Abcam protocol<sup>45</sup> was employed after slight modifications (details in the ESI). Intensity was measured at an excitation wavelength of 488 nm and at an emission wavelength of 535 nm for 12 hours using a fluorescence microplate reader.

### 2.6. Statistical analysis

The data were analyzed by student's t-test using MATLAB. Differences between means were considered statistically significant at  $p < 0.05$ . Data are presented as mean  $\pm$  standard error of the mean (SEM) for at least three independent experiments, unless otherwise stated. T-test analysis was performed to detect the differences between kinetic parameters of control bacteria and AgNPs-exposed bacteria as well as the differences between toxicity effects of nanoparticles on the resultant culture of bioreactors (control bacteria and AgNPs-exposed bacteria). Also, the changes in negative charge of the nanoparticle surface in different solutions were assessed by t-test analysis.

## 3. Results and Discussion

### 3.1. Bacterial growth

Fig. 1 shows the evolution of the OD600 inside the bioreactors.

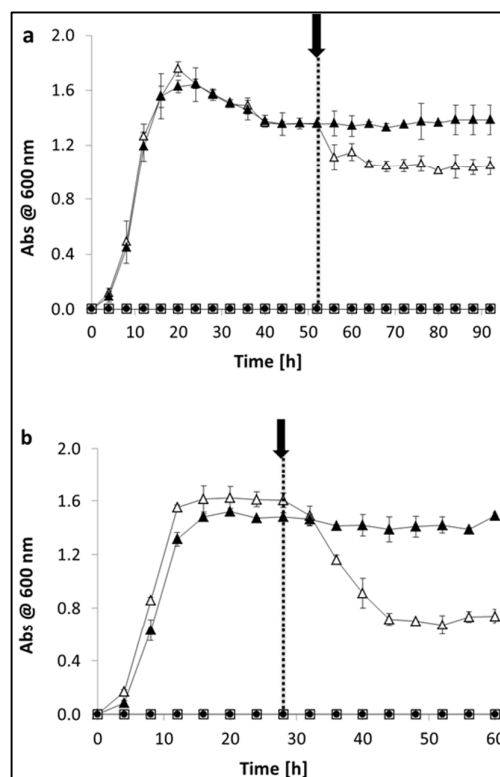


**Fig. 1** Effect of continuous injection of AgNPs [1 mg/L] on *E. coli* growth at two specific growth rates in continuous culture. (a) 0.1 h<sup>-1</sup> and (b) 0.2 h<sup>-1</sup>. ▲ bacteria without AgNPs, Δ bacteria exposed to AgNPs. ● M9 media in absence of bacteria or AgNPs. □ M9 media and AgNPs. The arrow and dashed line show time when AgNPs injected. Bars represent the error between duplicates reactors.

Fig. 1 shows that at both conditions blank vessels maintain a value of zero, indicating a lack of contamination. As expected, at both growth conditions, all inoculated bioreactors reached steady state at similar times. After steady state was achieved, for each run, two bioreactors were used for the exposure condition (EB) while the other two were left undisturbed for control purposes. After AgNPs injection, there was a period in which biomass decreased for both exposed bioreactors at runs of 0.1 h<sup>-1</sup> and 0.2 h<sup>-1</sup>, however in both cases these bioreactors achieved a new steady state condition after 8 h and 16 h, for the 0.1 h<sup>-1</sup> and 0.2 h<sup>-1</sup> conditions, respectively. At the end of the experiments, the exposed bioreactor operating at 0.1 h<sup>-1</sup> (EB-0.1) showed a 15.4% lower concentration of bacteria compared to the control bioreactors operating at 0.1 h<sup>-1</sup> (CB-0.1). The reduction of bacteria concentration was 56.3% in the EB-0.2 reactors compared to CB-0.2. These results showed that at the conditions tested, microorganisms growing at a lower specific growth rate are less inhibited in term of biomass, compared to those growing at a higher growth rate. The total silver concentration in the blank bioreactors (M9, no bacteria) was very close to 1 mg/L (Figure S5 in the ESI). However, in all exposed bioreactors the concentration of AgNPs was lower than the desired value due to possible trapping in the pellets of bacteria during the centrifugation step of the sampling process.

### 3.2. Kinetic parameters determination

Table 1 shows the concentration of bacteria inside the bioreactors ( $X$ ), concentration of glucose inside the bioreactors ( $S_{out}$ ), saturation constant ( $K_s$ ), yield coefficient ( $Y_{x/s}$ ), maximum yield coefficient ( $Y_{max}$ ), and maintenance coefficient ( $m_s$ ). All details of kinetic parameters determination are included in the ESI.

**Table 1** Kinetic parameter of *E. coli* at 0.1 h<sup>-1</sup> and 0.2 h<sup>-1</sup> for exposed and control bioreactors

Kinetic Parameter	Control $\mu = 0.1 \text{ h}^{-1}$	Control $\mu = 0.2 \text{ h}^{-1}$	Exposed $\mu = 0.1 \text{ h}^{-1}$	Exposed $\mu = 0.2 \text{ h}^{-1}$
$X$ (mg cell/L)	1.06±0.05	0.62±0.02	0.7±0.01	0.29±0.01
$S_{out}$ (mmol/L)	0.78±0.036	21.04±0.8	1.38±0.03	28.24±0.26
$S_{consumed}$ (mmol/L)	43.22±0.04	22.96±0.8	42.62±0.03	15.76±0.26
$K_s$ (mmol/L)	0.84±0.03	0.84±0.03	1.53±0.03	1.53±0.01
$\mu$ (h <sup>-1</sup> )	0.1	0.2	0.1	0.2
$Y_{x/s}$ (mg cell/mmol S consumed)	0.025±0.0012	0.027±0.002	0.016±0.0003	0.018±0.0015
$Y_{max}$ (mg cell/mmol S consumed)		0.03		0.02
$m_s$ (mg cell/mmol S consumed.h <sup>-1</sup> )		0.737		1.146

After the injection of AgNPs,  $K_s$  for the exposed bioreactors (EB-0.1 and EB-0.2) increased 82% compared to their respective controls (CB-0.1 and CB-0.2).  $K_s$  for EB-01 and EB-0.2 were the same because the concentration of AgNPs in both cases was the same, which agree with kinetic inhibitory models. These results agreed with Bhattacharya and Mukherjee,<sup>46</sup> who reported that the inhibition of sugar metabolism was due to the inactivation of the phosphomannose isomerase enzyme in the bacteria because of their interaction with the AgNPs.

Both EB-0.1 and EB-0.2 had a significant reduction in the yield coefficient ( $Y_{x/s}$ ) compared to their respective controls ( $p = 0.01$  and  $p = 0.001$ , respectively).

An increase in the maintenance coefficient for EB cultures was detected. In addition, the maximum biomass yield for EB cultures decreased ~33% compared to the controls. The decrease in  $Y_{max}$  in the EB was attributed to the increase in  $m_s$ . The maintenance coefficient ( $m_s$ ) depends partially on the cellular requirements for osmoregulation,<sup>47</sup> and these results showed that chronic exposure to the AgNPs can affect cell requirements. The changes of  $Y_{max}$  with specific growth rate in continuous systems were similar to those obtained at different times in batch cultures.<sup>48</sup> These results demonstrated the different effects on the cells' physiology and regulatory pathways when the tests were performed in both batch and continuous systems.<sup>48</sup> This highlighted the difficulties involved in interpreting the data and drawing general conclusions when using different bioreactor configurations.

### 3.3. Nanoparticles-ES interactions

**3.3.1. Effect of growth conditions on particle size and zeta potential.** The hydrodynamic diameters of the AgNPs in pristine M9 minimal medium and in the ES of the exposed bacteria were measured at 32 hours for both growth rates conditions (Table S5 in the ESI). Also, the stability of the AgNPs in distilled water (DI) was determined as a control (Figure S7 in the ESI). These results showed that ES reduced the stability of the nanoparticles in terms of size and zeta potential for both tested growth rate conditions. Major changes were observed at the EB-0.1 bioreactor where the lower zeta potential values of the AgNPs were detected ( $p = 0.0001$ ) in comparison to EB-0.2. This can be explained by the attachment of the protein corona to the surfaces of the nanoparticles as reported by Shannahan *et al.*<sup>49</sup> Since the biomass evolution profiles of the EB-0.1 cultures were less inhibited by the AgNPs, Cryo-TEM images were only collected for this condition (Fig. 2).

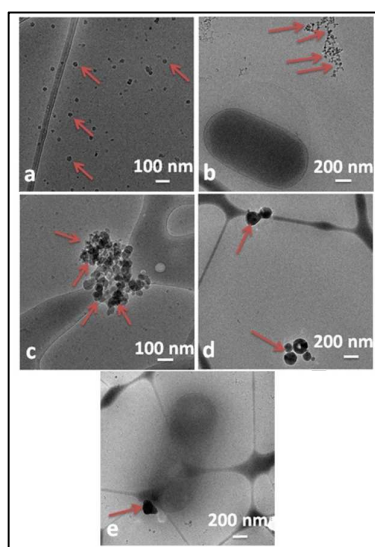


**Fig. 2** Cryo-TEM images of bacteria- nanoparticles interaction, ES- nanoparticles interaction, and protein corona formation on nanoparticles surface from exposed bioreactor operating at  $0.1\text{h}^{-1}$  (EB-0.1) after 8 hours and 32 hours after dosing of nanoparticles started. (a) AgNPs in DI water. (b) Released ES with trapped nanoparticles inside after 8 hours from dose. (c) Magnified ES-nanoparticles interactions from (a). (d) AgNPs-ES complex after 32 hours from starting dose showing large size distribution. (e) AgNPs-ES complex outside cell prevented from penetration. Red arrows represent nanoparticles.

For reference, images of AgNPs in DI water were also collected (Fig. 2). ES from EB-0.1 images showed that the nanoparticles were trapped in the ES after 8 hours in the bioreactor (Fig. 2b). The images also showed that agglomeration increased after 32 hours at EB-0.1 (Fig. 2c). These results suggested that nanoparticle-ES interactions can lead to biological corona formation on the surfaces of the nanoparticles due to the high affinity of the nanoparticle surface with sulfur- or nitrogen-containing compounds, especially amino acids.<sup>21</sup> Since protein corona is an unstable form of assembly on the surfaces of the nanoparticles,<sup>50,51</sup> different AgNPs sizes can be observed in Fig. 2d. Therefore, the surface of the AgNPs had been modified and these nanoparticles could not pass through cell membranes (Fig. 2e).

**3.3.2. Formation of protein corona on the surfaces of the nanoparticles.** Protein conformation of  $\alpha$ -helices and  $\beta$ -sheets were examined in samples collected from EB-0.1, CB-0.1 and EB-0.2, CB-0.2 at 8 hours and 32 hours. The applied lower and upper limit of frequency for deconvolution of main peaks for  $\alpha$ -helix and  $\beta$ -sheets was  $1600\text{ cm}^{-1}$  and  $1700\text{ cm}^{-1}$ . For this purpose, the applied range of frequency for  $\alpha$ -helical was between  $1715\text{--}1685\text{ cm}^{-1}$  and the applied frequency range for  $\beta$ -sheets was between  $1640\text{--}1615\text{ cm}^{-1}$ .<sup>52</sup> Fig. 3 shows that the ratio of the area representing  $\beta$ -sheets to the area of  $\alpha$ -helix was  $< 1$  for all conditions except AgNPs in ES from EB-0.1. At the EB-0.1 condition, the ratio values of  $\beta$ -sheets integral to  $\alpha$ -helix integral were 3.1 and 2.4, at 8 hours and 32 hours, respectively. This suggests that the nanoparticles induced a

reduction of protein content in the  $\alpha$ - helix or enhanced the conformational entropy of the protein.<sup>2,36</sup>

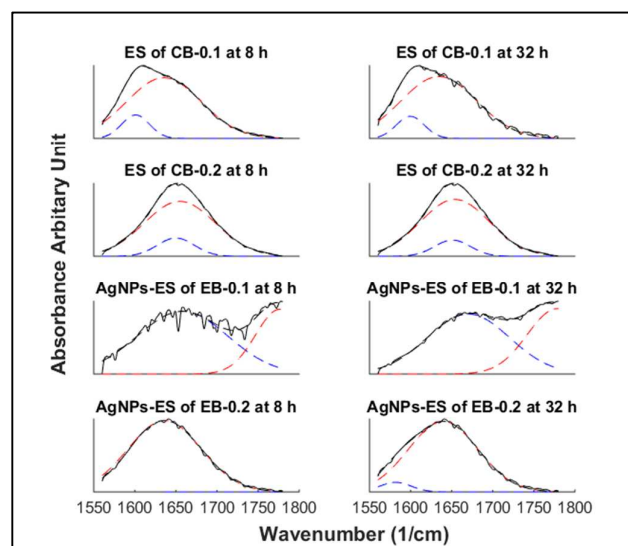


**Fig. 3** FTIR spectra of  $1800\text{--}1550\text{ cm}^{-1}$  region for ES released by control bacteria as well as obtained ES from AgNPs exposed bacteria for both specific growth rates. Black lines present the raw spectra of protein regions of ES. Blue and red lines show the area under  $\beta$ -sheet structures and  $\alpha$ -helix structures of proteins in ES, respectively.

HCA of FTIR data from ES composition showed that ES extracted from EB-0.1 segregated distinctly from the ES of the control groups at  $0.2\text{ h}^{-1}$  (Figure S10 in the SI). Therefore, the formation of protein corona on the surface of AgNPs depended on the composition of ES released by bacteria at different specific growth rates.

TGA was conducted (weight loss vs. temperature) to determine thermal stability of the ES that were interacting with the AgNPs. The analysis was performed using derivative thermogravimetric analysis (DTG) from the TGA results. The thermal stability of the ES at CB-0.1 showed a double peak at DTG, which exhibited a 30% weight loss at  $100\text{ }^{\circ}\text{C}$  followed by a minor peak at  $300\text{ }^{\circ}\text{C}$  with less than a 5% weight loss (Fig. 4a) and (Figure S11a in the ESI). In addition, DTG of AgNPs-ES at EB-0.1 (Fig. 4a) showed a major peak at  $100\text{ }^{\circ}\text{C}$  to  $200\text{ }^{\circ}\text{C}$  associated with a 20% weight loss, and this was followed by a minor peak at  $400\text{ }^{\circ}\text{C}$  with a less than 10% weight loss. On the other hand, ES at CB-0.2 had a double peak with 20% weight loss at  $100\text{ }^{\circ}\text{C}$  and  $220\text{ }^{\circ}\text{C}$  (Fig. 4b). However, AgNPs-ES at EB-0.2 (Fig. 4b) had two more minor peaks with 2% weight loss that were observed at  $450\text{ }^{\circ}\text{C}$  to  $550\text{ }^{\circ}\text{C}$ . This was in addition to the peaks at  $100\text{ }^{\circ}\text{C}$  to  $180\text{ }^{\circ}\text{C}$  and  $220\text{ }^{\circ}\text{C}$  with a 12% weight loss. Thermograms at  $700\text{ }^{\circ}\text{C}$  indicated that the AgNPs had the lowest weight loss at EB-0.1, while the ES had their maximum weight loss due to the degradation of protein at the higher temperatures.

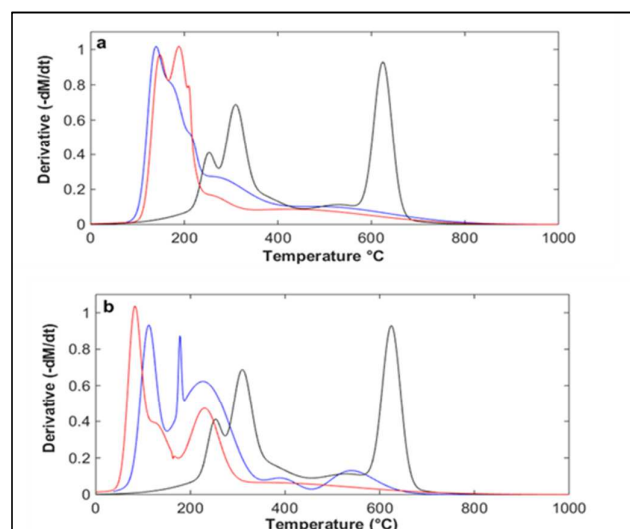


**Fig. 4** Derivative thermogravimetric (DTG) curves of AgNPs, ES-AgNPs, and ES. (a) First derivative of thermal stability of AgNPs-ES from EB-0.1 and ES of CB-0.1, and (b) First derivative of thermal stability of AgNPs-ES from EB-0.2 and ES of CB-0.2. Thermal stability of AgNPs-casein was obtained as a reference to compare with interacted AgNPs-ES. Black, blue, and red lines represent AgNPs, AgNPs-ES, and ES, respectively. Data were also obtained by taking the first derivative of the TGA lines. Raw data of TGA were smoothed by a moving average and the Gaussian fit to first derivative of smooth data has been found by MATLAB software.

These results supported the results obtained by ATR-FTIR, which indicated that the AgNPs-ES of EB-0.1 contained proteins<sup>53</sup> from the ES. At EB-0.2, the nanoparticles in the ES were impacted to a lesser extent compared to those in EB-0.1. This could have been due to the concentration and compositional differences of the ES produced at two growth conditions. ES from EB-0.1 formed protein corona, and surface properties changed after 32 hours, which resulted in a negative surface charge (Table S5 in the ESI) and a change in the size of the AgNPs (Figure S8 in the ESI). However, it was evident that no protein corona was formed at EB-0.2 (Fig. 3). The protein corona formed at EB-0.1 increased the size of the nanoparticles and decreased the penetration of nanoparticles into the cells. These results show the importance of electrostatic and hydrophobic interactions in the formation of the protein corona, and their biological and toxicological implications.

#### 3.4. Gene expression level at two specific growth rates

The results of the analyses indicated that there were several mechanisms by which bacteria responded to AgNPs exposure at both specific growth rates. The results, including various quantities of ES and their compositional characteristics as well as the AgNPs-ES interaction at different specific growth rates, indicated the necessity of investigating both specific growth rates for the gene expression level of eight target genes (*ompF*, *cueO*, *cusA*, *soxS*, *cpsB*, *zwf*, *copA*, and *fabR*), which were normalized using an internal reference gene, *rrsB* (Fig. 5).

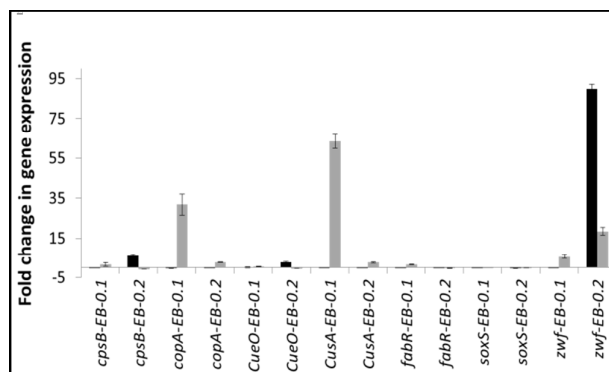


**Fig. 5** Quantitative amplification data of the target genes from continuous bioreactor products in response to AgNPs. Black and grey marks represent samples at 8 hours and 32 hours, respectively after continuous injection of AgNPs. Fold change in gene expression is relative to non-exposed control. Gene expressions were normalized against internal reference gene, *rrsB*. The error bars are the standard error of the mean of three technical replicate from two bioreactors at the same condition

In this study, the membrane in EB was protected by the response of up-regulated genes, such as *copA* and *cusA* to AgNPs at both specific growth rates. These genes are responsible for the silver and copper efflux of the membrane transporter, lipid biosynthesis, and the silver-translocating P-type ATPase efflux pump. Nanoparticles mediate the generation of ROS and also modulate the antioxidant activities of ROS-metabolizing enzymes, such as slow electron transport, the NADPH-dependent flavin enzyme, catalase, glutathione peroxidase, and superoxide dismutase.<sup>37</sup> In general, the *soxS* and *cueO*<sup>21,37</sup> genes, which are responsible for ROS expression, were not affected by the AgNPs at EB-0.1. Only *cueO* genes were up-regulated at EB-0.2. Also, the *zwf* gene showed a higher expression at EB-0.2 in comparison with EB-0.1, which may be associated with changes in the metabolic pathway of glucose-6-phosphate dehydrogenase in the respiration process<sup>37</sup> and/or the relatively impenetrable membrane of EB-0.1.<sup>54</sup> At EB-0.1, the nanoparticles did not cause the generation of ROS, and as such the cells were not involved in compensating for the disruptive impacts of the nanoparticles due to the formation of ROS. However, the activation of *copA*, *cpsB*, *fabR*, and *cusA* regulons prevented irreversible damage to EB-0.1.

#### 3.5. Comparison of cultures to acute exposure to AgNPs

Since the continuous culture results showed different responses at the two specific growth rates, we compared the response of the resultant culture at these two conditions to acute exposure to nanoparticles in terms of respiration activity, membrane permeation, and intracellular ROS production. These tests were performed in batch conditions using the resultant cultures from the control bioreactors (CB) and exposed bioreactors (EB). In addition, no nanoparticles for the negative control and 10 mg/L for the positive control were applied for the inhibitory effect of AgNPs.

**3.5.1. Inhibitory effect on respiration.** Fig. 6 shows no differences between the percent of remaining respiration (PRR) of EB and CB groups at both specific growth rates ( $p > 0.05$ ) when they were exposed to different nanoparticle

## ARTICLE

concentrations. Silver ions released from the nanoparticles are the main mechanism for metabolic disruption of bacteria. These results showed that at batch growing conditions, the resultant cultures respond similarly to nanoparticle exposure.

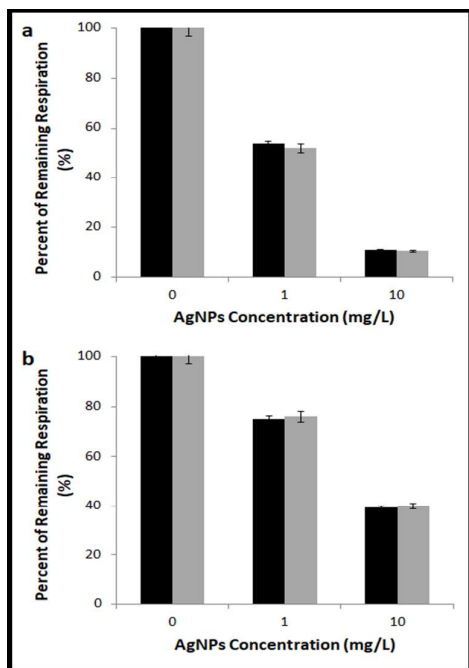


**Fig. 6** Represents percent of remaining respiration (PRR) of continuous bioreactor products including AgNPs-exposed bioreactor (EB) and control bioreactor (CB) under AgNPs (1 mg/L, and 10 mg/L). a) PRR values of CB and EB of 0.1 h<sup>-1</sup>, and b) PRR values of CB and EB of 0.2 h<sup>-1</sup>. Black marks show CB and gray marks represent EB. Each value represents an average of 6 wells from two duplicate 96 well microplates.

**3.5.2. Inhibitory effect on membrane permeation.** The undisturbed cell membrane (UCM) results shown in Fig. 7 indicate that the inhibitory effect of the AgNPs (1 mg/L) on EB after exposure to AgNPs at both 0.1 h<sup>-1</sup> and 0.2 h<sup>-1</sup> was lower than that of CB exposed to AgNPs. The statistical analysis confirmed that low concentrations (1 mg/L) of the AgNPs had a higher inhibitory effect on the CB at 0.1 h<sup>-1</sup> and 0.2 h<sup>-1</sup> than they had on EB-0.1 and EB-0.2 ( $p = 0.09$  and  $p = 0.02$ , respectively). Shokri *et al.*<sup>54</sup> reported that the cyclic fatty acids of *E. coli* were increased at lower growth rates. Hence, the mechanical strength of the cell membranes showed high resistance to sonication and osmotic shock/enzymatic treatment.<sup>54</sup> In comparison to a previous study,<sup>1</sup> a slight high inhibitory effect was observed at a low AgNPs (1 mg/L) concentration and there was no physical damage to the bacteria at high concentrations of AgNPs (15 mg/L and 50 mg/L). This was due to the aggregation of the AgNPs at high concentrations and the decreased steric forces due to the release of ES during bacteria metabolism.<sup>1</sup>

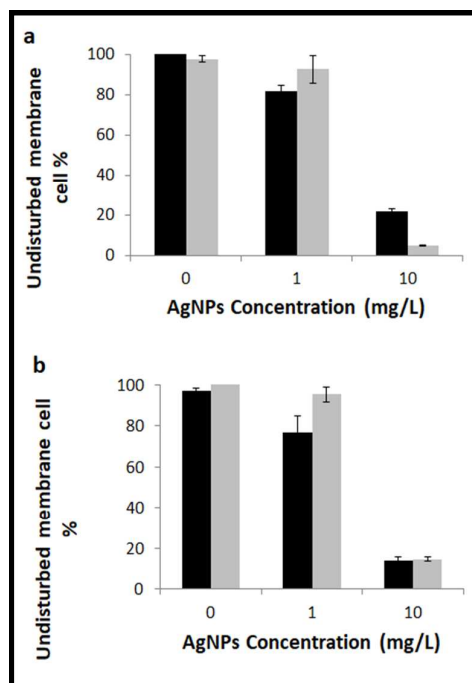


**Fig. 7** Represents undisturbed cell membrane (UCM) of continuous bioreactor products including AgNPs-exposed bioreactor (EB) and control bioreactor (CB) under AgNPs (1 mg/L, and 10 mg/L). UCM values were measured at 5 hours a) CB and EB of 0.1 h<sup>-1</sup>, and b) CB and EB of 0.2 h<sup>-1</sup>. Black marks show CB and gray marks represent EB. Each value represents an average of 6 wells from two duplicate microplates.

**3.5.3. Evaluation of the generation of ROS.** When CB-0.1 was exposed to 1 mg/L of AgNPs, the fluorescence increased, and the exposure of EB-0.1 to AgNPs (1 mg/L) show significant generation of ROS ( $p < 0.05$ ) (Fig. 8a). Fig. 8b shows that the level of fluorescence was not statistically different between the CB-0.2 and EB-0.2 after exposure to 1 mg/L of AgNPs ( $p = 0.93$ ). The resultant cultures from EB and CB bioreactors have different responses to acute exposure to nanoparticles in terms of membrane permeation and ROS formation for both specific growth rates. Significant ROS generation and UMC were observed between CB and EB, which contrast with PRR between CB and EB in the same condition. This suggested that ROS generated during electron transport is slowed by high mitochondrial membrane potential.<sup>55</sup> Hence, oxygen radicals react with oxygen dissolved in the membrane and cause the membrane disruption.

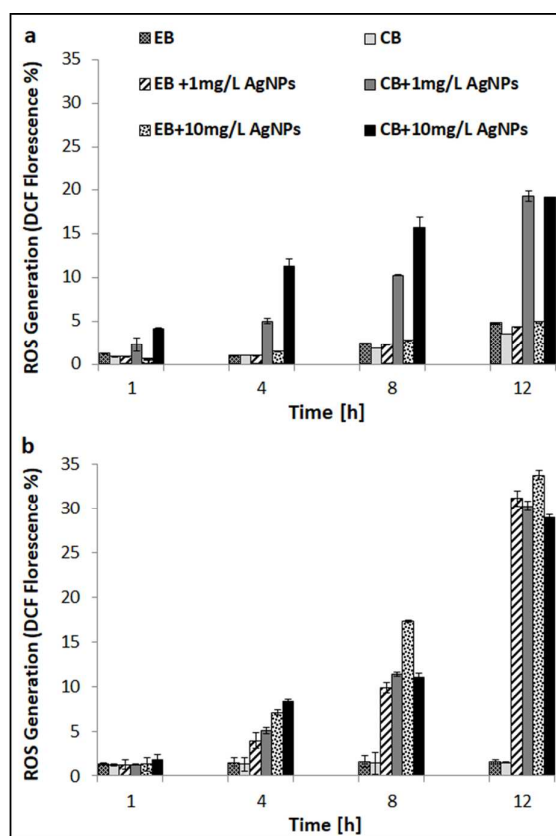


Fig. 8 Represents reactive oxygen species level (ROS) of bioreactor culture products for exposed bioreactor (EB) and control bioreactor (CB) contacted with AgNPs (1 mg/L, and 10 mg/L). ROS generation value in a) CB and EB of 0.1 h<sup>-1</sup>, and b) CB and EB of 0.2 h<sup>-1</sup>. Each value represents an average of 6 wells from two duplicates 96 well microplates.

### 3.6. Discussion

In terms of AgNPs impacts on kinetic parameters, our results showed that the microbial population continues to grow in the presence of the AgNPs, however, metabolic activity is impaired. This is demonstrated by changes in the kinetic parameters (decrease of  $Y_{x/s}$  and  $Y_{max}$  as well as increase of  $K_s$  and  $m_s$ ). The metabolic changes led to a new steady state for a continuous culture in which the resultant concentration of biomass is lower than that obtained at the steady state in non-exposed conditions. Thus, the resultant biomass concentration was inversely dependent on the specific growth rate (high specific growth rate, low end biomass concentration).

Kinetic parameter analysis helps us to understand the fate of the microbial population as a whole, but it does not provide insight into the mechanism(s) governing the observed effect. As such, bio-macromolecule analysis was utilized to elucidate the phenomena. The results from the AgNPs-ES interaction showed that different compositions of ES were produced at the two tested conditions (0.1 h<sup>-1</sup> and 0.2 h<sup>-1</sup> specific growth rate). The concentration of extracted ES from the continuous culture was quantified and normalized to the OD600 bacteria concentration (Figure S9 in the ESI). In general, the

concentration of ES at 0.1 h<sup>-1</sup> was higher than 0.2 h<sup>-1</sup>. After nanoparticle injection, the concentration of ES at EB-0.1 slowly increased until 32 hours. At EB-0.2, a temporary spike in ES concentration was observed at between 8 and 16 hours after AgNPs injection, however, this concentration sharply decreased by the end of the experiment. These findings agreed with Williams and Wimpenny<sup>8</sup> who reported that ES production decreases with an increase in the specific growth rate. An increase in ES due to nanoparticles was also observed by Zhang *et al.* using mixed cultures.<sup>56</sup>

Notably, the ES composition of the AgNPs-exposed bioreactors were different than the controls at the same condition as evidenced by the hierarchical cluster analysis of FTIR data (HCA, Figure S10 in the ESI). This study supports the idea that changes on the surface properties of AgNPs, at the two culture conditions, were due the production and excretion of ES with different compositions at the two specific growth rates tested. These varieties of ES composition were demonstrated by the TGA analysis. The TGA results for the AgNPs-ES complexes obtained from EB-0.1 supported the evidence regarding protein corona formation on the surface of the AgNPs. Li *et al.*<sup>7</sup> reported that total cellular polysaccharide (combination of ES and intracellular polysaccharide) decreased as the specific growth rate increased, while protein concentration increases. This was in agreement with the TGA result regarding the increase in protein of AgNPs-ES at EB-0.1. Moreover, FTIR showed that the ratio of the area representing  $\beta$ -sheets to the  $\alpha$ -helix of AgNPs-ES at EB-0.1 was higher than EB-0.2, which was induced due to the increase in  $\beta$  sheet content or due to the fortification of the conformational entropy of the protein at EB-0.1.<sup>2,36</sup> These results showed that *E. coli* produces more effective ES in terms of nanoparticles destabilization at lower specific growth rates.

In the context of transcriptomic analysis, the main genes that respond to chronic levels of continuous stress due to the nanoparticles are *zwf*, *CusA*, and *copA*. Specifically, the up-regulation of the *zwf* and *copA* genes was in agreement with the changes in growth parameters such as  $K_s$ ,  $Y_{max}$  and  $m_s$  in the exposed bioreactors. The *zwf* gene could lead to a  $K_s$  increase, while decreasing  $Y_{max}$ , in two ways, inactivation of phosphomannose by the AgNPs, and a drop in the efficiency of sugar metabolism.<sup>46</sup> The *copA* gene in the exposed cultures translocated silver thru the ATPase efflux pump by increasing  $m_s$ . Furthermore, the upregulation of the *cpsB* gene, production of capsular polysaccharide and canonical regulatory transcription,<sup>42</sup> was faster at EB-0.1 than EB-0.2, which showed a faster metabolic pathway response to the stressors for cultures growing at lower specific growth rates.<sup>32</sup> These results are evidence that cell requirements increase due to chronic exposure to AgNPs.

Finally, the acute test results showed that even if bacteria are able to adapt to nanoparticles, they cannot transfer this adaptability to the following generations over 114 generations at 0.2 h<sup>-1</sup> (number of *E. coli* generation during 32 hours of nanoparticles exposure). However, at 0.1 h<sup>-1</sup>, the number of generations was 206, which increases the probability of bacterial adaptation to nanoparticles, which was in agreement

with the acute tests. In this content, UCM and ROS generation between CB and EB showed that at a EB condition, nanoparticles did not significantly disrupt the cell membrane, and did not produce oxidative damage by ROS. Hence, EB are not compensating for a lower disruptive effect from nanoparticles than CB when they are exposed to nanoparticles of 1 mg/L. However, the low PRR for the 0.1 h<sup>-1</sup> resultant culture when exposed to AgNPs indicates the impact of culturing conditions on the bacterial response to AgNPs. Bacteria in a continuous culture caused the reduction in the inhibitory effect of AgNPs by producing ES, especially at 0.1 h<sup>-1</sup>. Therefore, the higher expression of the *zwf* gene at EB-0.2 in comparison with EB-0.1 was associated with the relatively modified surface chemistry of nanoparticles in EB-0.1 in a continuous culture. Hence, the PRR between CB and EB showed that the changes observed were a phenotypic response to the stress conditions and not permanent changes in the bacterial respiration mechanism. Wang *et al.* reported on the highly conserved nature of bacteria, which protect them from change through only a few genetic mutations.<sup>57</sup> This study is in agreement with the results obtained from the higher growth rate condition. However, another study claimed that genomic analysis of AgNPs exposed *E.coli* showed resistance by generation 200, where three mutations smoothly occurred in AgNPs resistance bacteria<sup>9</sup>.

These studies indicate that despite previous claims to the contrary, bacteria can easily evolve resistance to AgNPs, and this occurs by relatively simple genomic changes in a few generations. In conventional batch tests, since the contact time was 5 hours, the number of generations that were exposed to nanoparticles was 17, which means that at a batch culture condition the probability of adaptation is even lower than that for a continuous culture, unless the specific growth rates of a culture are high enough to decrease the number of generations. Hence, at lower specific growth conditions, the probability of producing nanoparticle-resistant bacteria will increase. Therefore, the bacterial culture condition influences the inhibitory effect of nanoparticles by changing their physiochemical properties, and also caused permanent bacterial resistance.

## Conclusions

The fate of nanoparticles and their inhibitory effects in a continuous culture depends on the bacterial specific growth rate associated with different concentrations and the composition of ES produced at each growth condition. ES at a lower growth rate are more effective in reducing the inhibitory effect of the nanoparticles. This occurs thru consumption of ROS, immobilization of the nanoparticles, and the formation of protein corona on the surfaces of the nanoparticles. Cultures exposed to nanoparticles are able to grow and achieve new stable conditions (steady state) at a higher maintenance coefficient than unexposed cultures. This is due to the activation of several regulons, such as *zwf*, *CusA*, and *copA*, which occurs to prevent irreversible damage from the stress condition.

## Conflicts of interest

The authors declare no conflicts of interest.

## Acknowledgements

This work was supported by the National Science Foundation under the grant numbers CBET-1350789 and CBET-1055652. The authors would like to appreciate Drs. D. Smith, E. Rubin from Graduate School of Oceanography and the URI Sequencing and Genomic Center.

## References

- 1 N. M. Anaya, F. Faghihzadeh, N. Ganji, G. Bothun and V. Oyanedel-Craver, *Sci. Total Environ.*, 2016, **565**, 841–848.
- 2 F. Faghihzadeh, N. M. Anaya, L. A. Schiffman and V. Oyanedel-Craver, *Nanotechnol. Environ. Eng.*, 2016, **1**, 1.
- 3 J. S. McQuillan, H. G. Infante, E. Stokes and A. M. Shaw, *Nanotoxicology*, 2012, **6**, 857–866.
- 4 A. Ivask, I. Kurvet, K. Kasemets, I. Blinova, V. Aruoja, S. Suppi, H. Vija, A. Käkinen, T. Titma, M. Heinlaan, M. Visnapuu, D. Koller, V. Kisand and A. Kahru, *PLoS ONE*, , DOI:10.1371/journal.pone.0102108.
- 5 K. Ikuma, A. W. Decho and B. L. T. Lau, *Front. Microbiol.*, , DOI:10.3389/fmicb.2015.00591.
- 6 E. Gulot, P. Georges, A. Brun, M. P. Fontaine-Aupart, M. N. Bellon-Fontaine and R. Briandet, *Photochem. Photobiol.*, 2002, **75**, 570–578.
- 7 M. Li, P. Nkrumah and M. Xiao, *Inland Waters*, 2014, **4**, 357–362.
- 8 A. G. Williams and J. W. T. Wimpenny, *J. Gen. Microbiol.*, 1978, **104**, 47–57.
- 9 J. L. Graves, M. Tajkarimi, Q. Cunningham, A. Campbell, H. Nonga, S. H. Harrison and J. E. Barrick, *Front. Genet.*, , DOI:10.3389/fgene.2015.00042.
- 10 Z. Fencel, J. Řičica and J. Kodešová, *J. Appl. Chem. Biotechnol.*, 1972, **22**, 405–416.
- 11 K. Kovárová-Kovar and T. Egli, *Microbiol. Mol. Biol. Rev. MMBR*, 1998, **62**, 646–666.
- 12 P. De Leenheer and N. G. Cogan, *J. Math. Biol.*, 2009, **59**, 563–579.
- 13 M. Lin, H. F. Huo and Y. N. Li, , DOI:10.1016/j.nonrwa.2012.02.016.
- 14 T. King, S. Seeto and T. Ferenci, *Genetics*, 2006, **172**, 2071–2079.
- 15 M. A. Radzig, V. A. Nadtochenko, O. A. Koksharova, J. Kiwi, V. A. Lipasova and I. A. Khmel, *Colloids Surf. B Biointerfaces*, 2013, **102**, 300–306.

- 16 Y. Chen, Z. Wang, M. Xu, X. Wang, R. Liu, Q. Liu, Z. Zhang, T. Xia, J. Zhao, G. Jiang, Y. Xu and S. Liu, *ACS Nano*, 2014, **8**, 5813–5825.
- 17 D. Fraser and M. Kaern, *Mol. Microbiol.*, 2009, **71**, 1333–1340.
- 18 W. Harder and L. Dijkhuizen, *Philos. Trans. R. Soc. Lond. B. Biol. Sci.*, 1982, **297**, 459–480.
- 19 H. Veldkamp and H. W. Jannasch, *J. Appl. Chem. Biotechnol.*, 1972, **22**, 105–123.
- 20 K. M. Peil and A. F. Gaudy, *Appl. Microbiol.*, 1971, **21**, 253–256.
- 21 J. S. McQuillan and A. M. Shaw, *Nanotoxicology*, 2014, **8**, 177–184.
- 22 *Escherichia coli* (Migula) Castellani and Chalmers ATCC® 700926&tr, <https://www.atcc.org/Products/All/700926.aspx#culturemethod>, (accessed February 6, 2017).
- 23 Y. Jiao, G. D. Cody, A. K. Harding, P. Wilmes, M. Schrenk, K. E. Wheeler, J. F. Banfield and M. P. Thelen, *Appl. Environ. Microbiol.*, 2010, **76**, 2916–2922.
- 24 S. Ganal, C. Gaudin, K. Roensch and M. Tran, *J Exp Microbiol Immunol*, 2007, **11**, 54–59.
- 25 G. Molin, *Eur. J. Appl. Microbiol. Biotechnol.*, 1983, **18**, 303–307.
- 26 R. M. Maier, I. Pepper and C. Gerba, *Environ. Microbiol.*, 2000, 43–59.
- 27 J. Glazyrina, E.-M. Materne, T. Dreher, D. Storm, S. Junne, T. Adams, G. Greller and P. Neubauer, *Microb. Cell Factories*, 2010, **9**, 42.
- 28 J. Monod, *Annu. Rev. Microbiol.*, 1949, **3**, 371–394.
- 29 S. J. Pirt, *Proc. R. Soc. Lond. B Biol. Sci.*, 1965, **163**, 224–231.
- 30 A. Xi and G. D. Bothun, *The Analyst*, 2014, **139**, 973–981.
- 31 S. R. Chowdhury, S. Manna, P. Saha, R. K. Basak, R. Sen, D. Roy and B. Adhikari, *J. Appl. Microbiol.*, 2011, **111**, 1381–1393.
- 32 J. Zeng, J.-M. Gao, Y.-P. Chen, P. Yan, Y. Dong, Y. Shen, J.-S. Guo, N. Zeng and P. Zhang, *Sci. Rep.*, 2016, **6**, 26721.
- 33 J. H. Ward, *J. Am. Stat. Assoc.*, 1963, **58**, 236.
- 34 C. Matthäus, B. Bird, M. Miljković, T. Chernenko, M. Romeo and M. Diem, *Methods Cell Biol.*, 2008, **89**, 275–308.
- 35 Q. Lin, C. Mao, A. Kong, X. Bu, X. Zhao and P. Feng, *J. Mater. Chem. A*, 2017, **5**, 21189–21195.
- 36 N. Durán, C. P. Silveira, M. Durán and D. S. T. Martinez, *J. Nanobiotechnology*, 2015, **13**, 55.
- 37 A. Baez and J. Shiloach, *Microb. Cell Factories*, 2013, **12**, 1.
- 38 J. McQuillan, .
- 39 K. Arunasri, M. Adil, K. Venu Charan, C. Suvro, S. Himabindu Reddy and S. Shivaji, *PLoS ONE*, 2013, **8**, e57860.
- 40 K. W. Kinzler, *Gene Expr.*, 1999, **270**, 484–487.
- 41 Z. Rahman, N. Rashid, J. Nawab, M. Ilyas, B. H. Sung and S. C. Kim, *Environ. Sci. Pollut. Res.*, 2016, **23**, 12007–12018.
- 42 G. Huang, D. Xia, T. An, T. W. Ng, H. Y. Yip, G. Li, H. Zhao and P. K. Wong, *Appl. Environ. Microbiol.*, 2015, **81**, 5174–5183.
- 43 M. W. Pfaffl, *Real-Time PCR*, 2006, **63**, 63–82.
- 44 N. M. Anaya, F. Solomon and V. Oyanedel-Craver, *Environ. Sci. Nano*, , DOI:10.1039/C5EN00074B.
- 45 DCFDA - Cellular Reactive Oxygen Species Detection Assay Kit (ab113851) | Abcam, <http://www.abcam.com/dcfda-cellular-reactive-oxygen-species-detection-assay-kit-ab113851.html>, (accessed February 6, 2017).
- 46 R. Bhattacharya and P. Mukherjee, *Adv. Drug Deliv. Rev.*, 2008, **60**, 1289–1306.
- 47 X. Wu, R. Altman, M. A. Eiteman and E. Altman, *Appl. Environ. Microbiol.*, 2014, **80**, 2880–2888.
- 48 J. H. Seo and J. E. Bailey, *Biotechnol. Bioeng.*, 1986, **28**, 1590–1594.
- 49 J. H. Shannahan, X. Lai, P. C. Ke, R. Podila, J. M. Brown and F. A. Witzmann, *PLoS ONE*, , DOI:10.1371/journal.pone.0074001.
- 50 M. Mahmoudi, I. Lynch, M. R. Ejtehadi, M. P. Monopoli, F. B. Bombelli and S. Laurent, *Chem. Rev.*, 2011, **111**, 5610–5637.
- 51 S. Lara, F. Alnasser, E. Polo, D. Garry, M. C. Lo Giudice, D. R. Hristov, L. Rocks, A. Salvati, Y. Yan and K. A. Dawson, *ACS Nano*, , DOI:10.1021/acsnano.6b07933.
- 52 Y. N. Chirgadze and N. A. Nevskaya, *Biopolymers*, 1976, **15**, 627–636.
- 53 M. M. Yallapu, N. Chauhan, S. F. Othman, V. Khalilzad-Sharghi, M. C. Ebeling, S. Khan, M. Jaggi and S. C. Chauhan, *Biomaterials*, 2015, **46**, 1–12.
- 54 A. Shokri, A. M. Sandén and G. Larsson, *Appl. Microbiol. Biotechnol.*, 2002, **58**, 386–392.
- 55 M. P. Murphy, *Biochem. J.*, 2009, **417**, 1–13.
- 56 C. Zhang, Z. Liang and Z. Hu, *Water Res.*, 2014, **50**, 350–358.
- 57 L. Wang, C. Hu and L. Shao, *Int. J. Nanomedicine*, 2017, **12**, 1227–1249.